Application of prospective ECG-triggered dual-source CT coronary angiography for infants and children with coronary artery aneurysms due to Kawasaki disease

[1]Y DUAN, MD, [2]X WANG, MD, PhD, [2]Z CHENG, MD, [2]D WU, MD and [2]L WU

[1]*Medical School of Shandong University, Shandong Medical Imaging Research Institute, Jinan, Shandong, China, and* [2]*Shandong Medical Imaging Research Institute, Shandong Provincial Key Laboratory of Diagnosis and Treatment of Cardio-cerebral Vascular Diseases, Jinan, Shandong, China*

Objectives: The aim of this study was to prospectively evaluate the initial application and value of prospective electrocardiogram (ECG)-triggered dual-source CT coronary angiography (DSCTCA) in the diagnosis of infants and children with coronary artery aneurysms due to Kawasaki disease.
Methods: 19 children [12 males; mean age 13.47 months, range 3 months to 5 years; mean heart rate 112 beats per minute (bpm), range 83–141 bpm] underwent prospective ECG-triggered DSCTCA with free breathing. Subjective image quality was assessed on a five-point scale (1, excellent; 5, non-diagnostic) by two blinded observers. The location, number and size of each aneurysm were observed and compared with those of transthoracic echocardiography (TTE) performed within 1 week. Interobserver agreement concerning the subjective image quality was evaluated with Cohen's κ-test. Bland–Altman analysis was used to evaluate the agreement on measurements (diameter and length of aneurysms) between DSCTCA and TTE. The average effective dose required for DSCTCA was calculated for all children.
Results: All interobserver agreement for subjective image quality assessment was excellent (κ=0.87). The mean $\pm$ standard deviation (SD) aneurysm diameter with DSCTCA was 0.76 $\pm$ 0.36 cm and with TTE was 0.76 $\pm$ 0.39 cm. The mean $\pm$ SD aneurysm length with DSCTCA was 2.06 $\pm$ 1.35 cm and with TTE was 2.00 $\pm$ 1.22 cm. The Bland–Altman plot for agreement between DSCTCA and TTE measurements showed good agreement. The mean effective dose was 0.36 $\pm$ 0.06 mSv.
Conclusion: As an alternative diagnostic modality, prospective ECG-triggered DSCTCA with excellent image quality and low radiation exposure has been proved useful for diagnosing infants and children with coronary artery aneurysms due to Kawasaki disease.
Advances in knowledge: Prospective ECG–triggered DSCTCA for infants and children allows rapid, accurate assessment of coronary aneurysms due to Kawasaki diseases, compared with TTE.

Received 17 November 2011
Revised 12 July 2012
Accepted 16 July 2012

DOI: 10.1259/bjr/18174517

Kawasaki disease (KD), also known as mucocutaneous lymph node syndrome, is an autoimmune vasculitis in which the small and medium vessels throughout the body become inflamed [1, 2]. It predominantly occurs in infants and children (younger than 5 years old). It affects many organ systems; injury, such as aneurysm, dilation, ectasia, stenosis and embolism, to the heart is rare but serious, and fatal myocardial infarction can be induced in untreated cases [3–6]. It is crucial to detect coronary artery lesions at an early stage [7]. Diagnosis of KD is based on clinical signs, symptoms and laboratory findings, but no specific laboratory test exists and it is hard to establish the diagnosis, especially in the early course [8].

Recently, multidetector CT, especially the advent of dual-source CT, has provided improved spatial and temporal resolution; moreover, multiple techniques on dose reduction have been applied in children. Electrocardiogram (ECG)-gated scans, especially retrospective ECG-gated scans, have been used to evaluate coronary artery lesions in children with KD [2, 9]. The high radiation dose required remains the main concern [10]; even though dose-saving methods including low tube potential, tube current modulation and body size-adapted CT protocols have been adopted, the effective radiation dose is still high at up to 2.17–3.14 mSv [11–13].

Recently, prospective ECG-triggered scans were considered to be the most promising approach for dose reduction as they were used in the assessment of cardiovascular deformities in children with congenital heart disease [14–17]; however, no further studies have been reported on the application of prospective ECG-triggered CT angiography in children with KD.

The aim of this study was to evaluate the initial application of prospective ECG-triggered dual-source CT coronary angiography (DSCTCA) in infants and children with coronary artery aneurysms due to KD.

Address correspondence to: Professor Ximing Wang, CT Department, Shandong Medical Imaging Research Institute, No. 324 Jingwu Road, Jinan, Shandong 250021, China. E-mail: wxming369@163.com

Methods and materials

Subjects

This study protocol was approved by the ethics board of our hospital. Written informed consent was obtained from all the children's parents.

22 consecutive first-visit children (age range 3 months to 5 years) with suspected coronary artery lesions due to KD were enrolled between December 2008 and January 2010 in our institute. There were 14 males (age range 3 months to 5 years) and 8 females (age range 8 months to 4 years and 7 months). General exclusion criteria for contrast-enhanced CT included known hypersensitivity to iodine-containing contrast media ($n=2$) and renal insufficiency (serum creatinine level $>150\,\mu mol\,l^{-1}$) ($n=1$).

A total of 19 children [12 males, 7 females; mean age 13.47 months, range 3 months to 5 years; mean weight 11 kg; mean heart rate 112 beats per minute (bpm), range 83–141 bpm] suspected of having coronary artery aneurysms due to KD were included in our study. All children underwent transthoracic echocardiography (TTE) within a week. The mean interval between the documented onset of KD and DSCTCA/TTE was 42 days (range 15–208 days), and the interval between the latest TTE and DSCTCA was 3 days (range 1–7 days). Low-dose prospective ECG-triggered DSCTCA with free breathing was performed in all children. Beta-blockers were not administered to any of the children.

The diagnosis was made according to the diagnostic criteria of the American Heart Association for coronary artery lesions in KD [8]. The risk stratification was established based on previous studies [1, 8]. All children received routine medical treatment, and underwent routine examinations including complete blood count, erythrocyte sedimentation rate, C-reactive protein and an ECG.

Scanning protocol

A prospective ECG-triggered CT angiography scan was performed on a DSCTCA scanner (SOMATOM® Definition; Siemens Healthcare, Forchheim, Germany) during free breathing. Sedation was achieved by administering oral chloral hydrate according to the patient's body weight and clinical condition. The scan range extended from the branching point of the trachea to the diaphragm.

Data were acquired according to the method described previously [15]. The data acquisition window was set at 40% of the RR interval. Data were acquired during every three or four heartbeats. The CT data acquisition duration was 3–5 s.

CT angiography acquisition with an automated bolus-tracking technique was initialised when enhancement in the ascending aorta exceeded 100 HU.

Contrast material injection protocol

The non-ionic iodinated contrast material (350 mg I ml^{-1}; Ultravist®; Schering, Berlin, Germany) was administered with a dual-chamber mechanical power injector (Stellant®; Medrad, Indianola, PA) via a 24-gauge cannula inserted into an antecubital vein. The contrast material dose was tailored to the individual's body weight (2 ml kg^{-1}) and was administered for a fixed duration injection protocol (20 s). We adopted a fixed duration injection protocol because fixed duration injections may allow a reduction in individual variability in aortic enhancement [18, 19]. After contrast injection, a given mass of saline chaser (half that of the contrast material) was administered at the same rate as the contrast material. The volume of the contrast material and the saline chaser was based on the results of one of our previous studies [15].

Image reconstruction and reformation

CT images were reconstructed in a monosegment mode with a slice thickness of 0.60 mm and reconstruction increment of 0.40 mm, using a medium smooth tissue convolution kernel (B26f). All images were transferred to an external workstation (Syngo®, Multimodality Workplace; Siemens Healthcare, Forchheim, Germany) for further image analysis.

Assessment of coronary artery lesions

The visualisation capability of coronary arteries was graded for 13 arterial segments [20], including 4 segments of the right coronary artery (RCA): proximal (RCA1), middle (RCA2), distal (RCA3) and posterior descending artery (PDA); 1 segment of the left main artery; 3 segments of the left anterior descending (LAD) artery: proximal (LAD1), middle (LAD2), distal (LAD3); 3 segments of the left circumflex (LCX) artery: proximal (LCX1), middle (LCX2), distal (LCX3); 1 segment of the diagonal branch (D); and 1 segment of the obtuse marginal branch (OMB). Subjective image quality was independently assessed by two radiologists, one with 5 years and one with 6 years of experience in reading coronary artery angiography images. Both readers were blinded to the patient-identifying information. Consensus agreement was achieved between the two observers if disagreement existed. Overall image quality was assessed using a five-point grading scale [12]: 1, no motion artefact (Figure 1a); 2, minimal motion artefact—one stair-step artefact (Figure 1b); 3, moderate motion artefact (Figure 1c)—>1 stair-step artefact or minimal blurring of a vessel; 4, severe artefact causing the blurring of a vessel and the assessment was limited (Figure 1d); 5, the vessel was not recognisable (Figure 1e). Grades 1–3 were considered sufficient for diagnosis. A coronary artery injury was diagnosed according to the following criteria [20–22]: coronary artery stenosis was defined as lumen narrowing ≥50%; an internal lumen diameter of a coronary artery segment enlarged to <1.5 times that of an adjacent normal segment was defined as a dilation; and an internal lumen diameter of a coronary artery segment larger than normal for age (normal coronary artery diameter ranges from 1 to 2 mm in newborns and infants) or enlarged to ≥1.5 times that of an adjacent normal segment was diagnosed as an aneurysm. When a coronary artery was larger than normal and without a segmental aneurysm, the vessel was considered ectatic.

The number, location and size of the detected coronary artery lesions and the presence or absence of intraluminal thrombosis and calcifications identified with DSCTCA or TTE was noted.

Echocardiography

TTE was performed by one echocardiographer with more than 10 years of experience in three-dimensional echo diagnostic imaging with a SONOS® 7500 ultrasound machine (SONOS 7500 Dimension, Philips Medical Systems, Bothell, WA) or a VIVID® 7 ultrasound machine (VIVID 7 Dimension, GE Healthcare, Waukesha, WI).

Radiation dose estimations of CT coronary angiography

The parameters relevant to radiation dose were obtained from the scan protocol generated by the CT system after each DSCTCA study. The parameters included scan length, CT volume dose index ($CTDI_{vol}$; mGy) and dose–length product (DLP; mGy · cm). The effective dose (mSv) from DSCTCA was derived by multiplying the DLP by a conversion factor of 2.5 (this was recommended by the manufacturer for paediatric examinations at 80 kV) to compensate for the adult-specific 32-cm phantom-based DLP value [23]. Then the DLP value was multiplied by the relevant conversion coefficient (k) for the chest of children: 0.039 mSv $(mGy \cdot cm)^{-1}$ for children younger than 4 months old, 0.026 mSv $(mGy \cdot cm)^{-1}$ for children between 4 months and 1 year old and 0.018 mSv $(mGy \cdot cm)^{-1}$ for children between 1 and 6 years old [14–17, 24, 25].

Statistical analysis

Statistical analysis was performed using an SPSS software package (SPSS for Windows, v. 17.0; Chicago, IL) and MedCalc software package (MedCalc for Windows, v. 11.0.0.0, MedCalc software, Mariakerke, Belgium). Continuous variables were expressed as the mean ± standard deviation and categorical variables as frequencies or percentages.

Interobserver agreement in subjective image quality grading and CT measurements was assessed by Cohen's

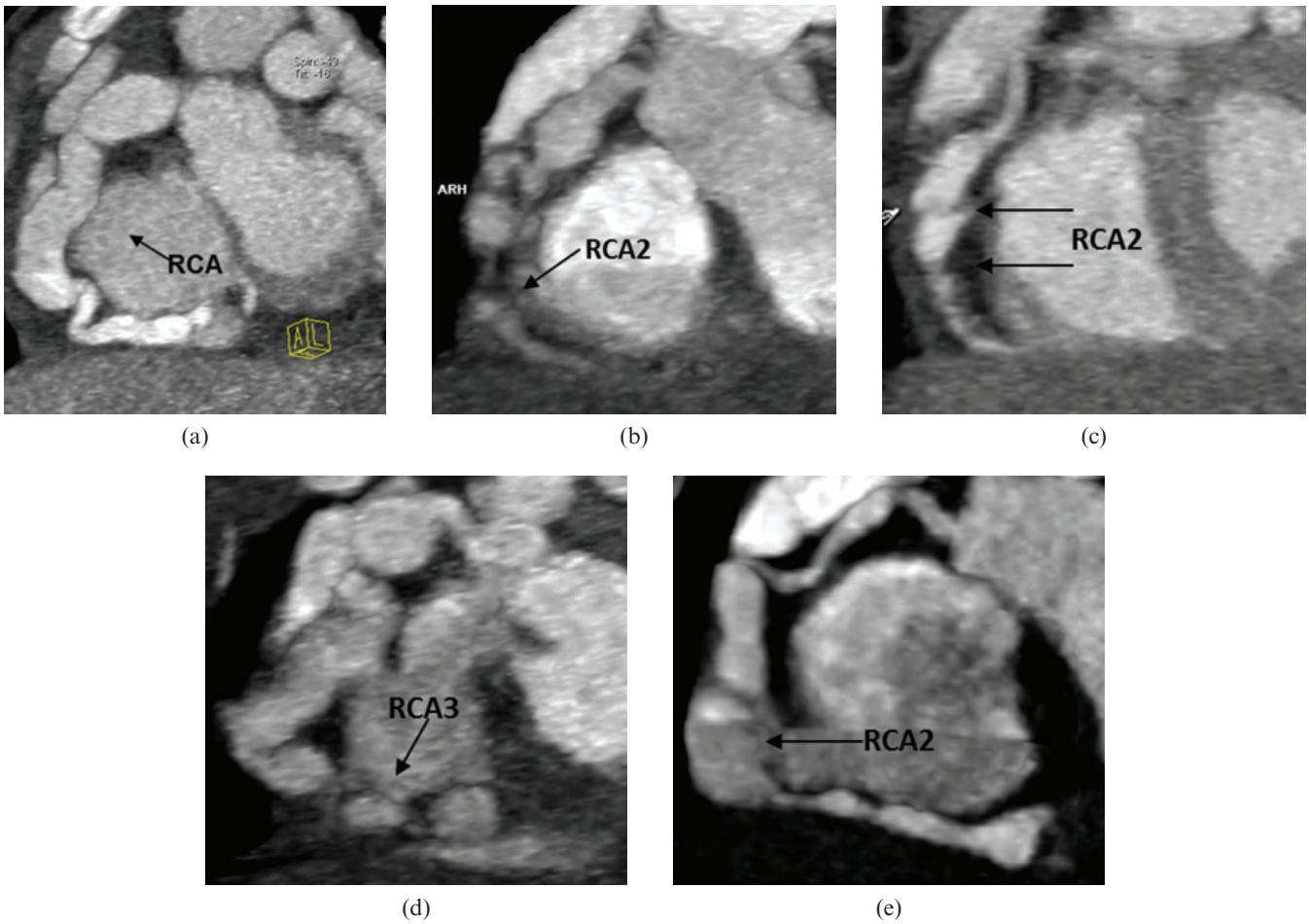

Figure 1. Maximum intensity projection images of the right coronary artery (RCA) in five different patients show the image quality score. (a) Score 1, no motion artefact was found in the whole RCA. (b) Score 2, minimal motion artefact was found in the RCA, middle segment (RCA2) (arrow). (c) Score 3, two stair-step artefacts were found in RCA2 (arrows). (d) Score 4, severe artefacts were found in the RCA, distal segment (RCA3) (arrow), and the assessment of RCA3 was limited. (e) Score 5, RCA2 cannot be identified because of marked motion artefact (arrow), but RCA3 was well delineated, so the image quality of RCA3 was rated as score 1.

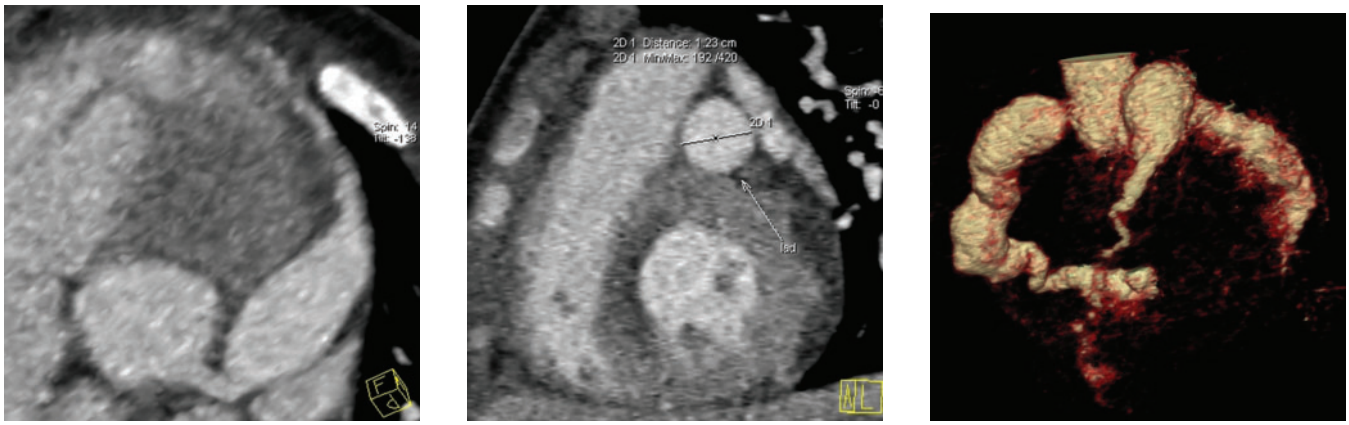

(a) (b) (c)

Figure 2. (a) Thin maximum intensity projection image showing the giant aneurysm in the left anterior descending artery, proximal segment (LAD1)+middle segment (LAD2). (b) The vertical section of the maximum aneurysm in the LAD artery showed that the maximum diameter of the aneurysm in the LAD artery is 1.23 cm. (c) Volume rendering image showing the cluster-like aneurysms in the right coronary artery and left circumflex artery, and the giant aneurysm in LAD1+LAD2.

κ-test [26], and κ-values of 0.61–0.80 corresponded to good agreement whereas values between 0.81 and 1.00 corresponded to excellent agreement. Bland–Altman analysis was used to evaluate the agreement on measurements (diameter and length of aneurysms) between DSCTCA and TTE. In Bland–Altman analysis, the mean values of the two examinations (x-axis) were plotted against the difference between the examinations (y-axis). A p-value <0.05 was considered statistically significant.

Results

All prospective ECG-triggered DSCTCA and TTE examinations were performed without technical problems, and the image quality was sufficient for data analysis in all cases; 15 patients were diagnosed with coronary artery lesions due to KD by both DSCTCA and TTE.

Dual-source CT coronary artery findings

A total of 21 aneurysms (Figure 2), 7 dilations and 11 arterial ectasias were detected by DSCTCA. Thrombosis was found in three aneurysms (Figure 3a) and three ectasias; calcification and stenosis were not detected by either DSCTCA or TTE. A total of 15 cases were classified as risk level IV by DSCTCA.

The interobserver agreement for subjective image quality was excellent (κ=0.87). The mean score of both observers for coronary artery segments was 1.6 ± 0.7. Diagnostic image quality was present in 91.5% (226/247) of the segments; non-diagnostic image quality was found at LCX3 in 3.2% (8/247) of the segments, at LAD3 in 1.6% (4/247) of the segments, at RCA3 in 0.08% (2/247) of the segments, at PDA in 0.04% (1/247) of the segments, at D in 1.2% (3/247) of the segments, at OMB in 0.08% (2/247) of the segments and at RCA2 in 0.04% (1/247) of the segments. 14 segments were graded as non-diagnostic owing to motion artefacts and 7 segments were graded as non-diagnostic because of lower CT attenuation.

The CT measurements showed excellent interobserver agreement (diameter, k=0.89; length, k=0.87).

Echocardiography findings

A total of 14 aneurysms, 5 dilations and 11 arterial ectasias were found by TTE. Thrombosis was found in three aneurysms (Figure 3b) and three ectasias. 13 out of 15 patients were classified as risk level IV, and 2 of them were classified as risk level III by TTE.

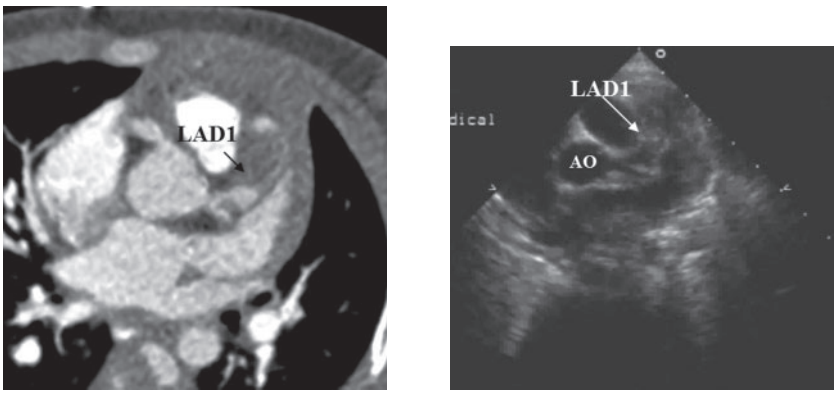

(a) (b)

Figure 3. (a) Maximum intensity projection image showing an aneurysm in the left anterior descending artery, proximal segment (LAD1), and a thrombus (arrow) is shown within the lumen of LAD1. (b) Parasternal short-axis view at the level of the aortic root (AO) demonstrates an aneurysm in LAD1 almost filled with thrombus (arrow).

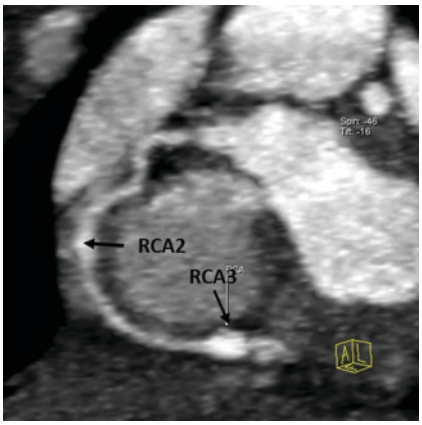

Figure 4. Thin maximum intensity projection images showing the circumscribed dilations in the right coronary artery (RCA), middle segment (RCA2), and a circumscribed aneurysm in the RCA, distal segment (RCA3); the aneurysm in the RCA2 was not detected by transthoracic echocardiography.

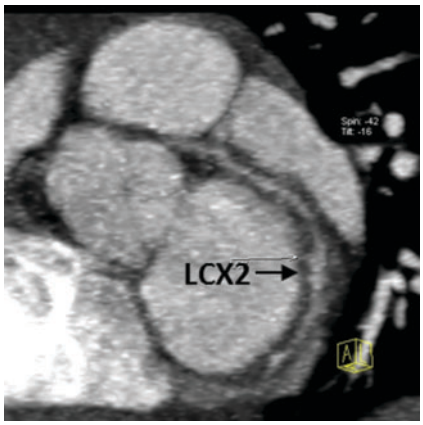

Figure 5. Thin maximum intensity projection images showing the circumscribed dilations in the left circumflex artery, middle segment (LCX2), which were not detected by transthoracic echocardiography.

TTE failed to detect seven aneurysms, with 2/7 in RCA3 (Figure 4, case 2), 1/7 in PDA, 1/7 in LAD2, 1/7 in LCX2, 1/7 in LCX3 and 1/7 in OMB. Two arterial dilations were also missed by TTE, one located in RCA2 (Figure 4) and one located in LCX2 (Figure 5).

Assessment of agreement between dual-source CT coronary angiography and transthoracic echocardiography

For all 14 aneurysms, 5 dilations and 11 ectasias detected by both DSCTCA and TTE, the described location and size were consistent with each other. The mean aneurysm diameter with DSCTCA was 0.76 ± 0.36 cm, and with TTE 0.76 ± 0.39 cm. Comparison of the mean diameters between DSCTCA and TTE yielded a bias of 2.4%, a lower limit of agreement of −29.3% and an upper limit of agreement of 34.1%. The Bland–Altman plot is shown in Figure 6a. The mean aneurysm length with DSCTCA was 2.06 ± 1.35 cm, and with TTE 2.00 ± 1.22 cm. Comparison of the mean lengths between DSCTCA and TTE yielded a bias of −2.0%, a lower limit of agreement of −25.1% and an upper limit of agreement of 21.2%. The Bland–Altman plot is shown in Figure 6b. The Bland–Altman plot for agreement between DSCTCA and TTE showed good agreement in the diameter and length measurements.

Radiation dose estimates

The conversion coefficients (k) for the chests of the children were age dependent; thus, the radiation dose was estimated for three age groups (Table 1). The mean $CTDI_{vol}$, DLP and effective dose of all 19 patients were 0.89 ± 0.33 mGy, 6.32 ± 2.33 mGy · cm and 0.36 ± 0.06 mSv (range 0.26–0.50 mSv), respectively.

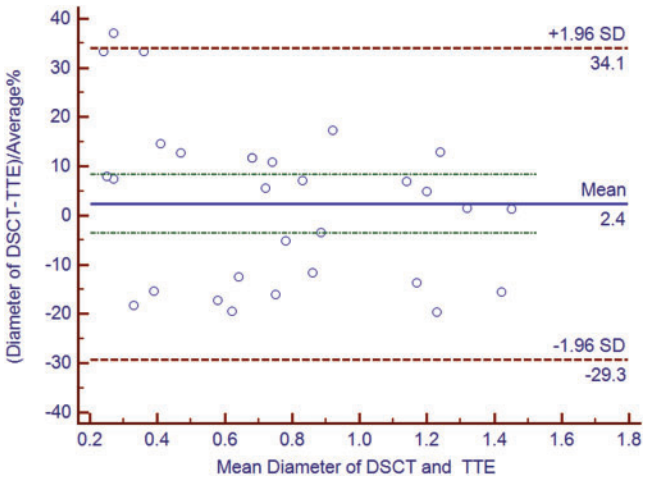

(a)

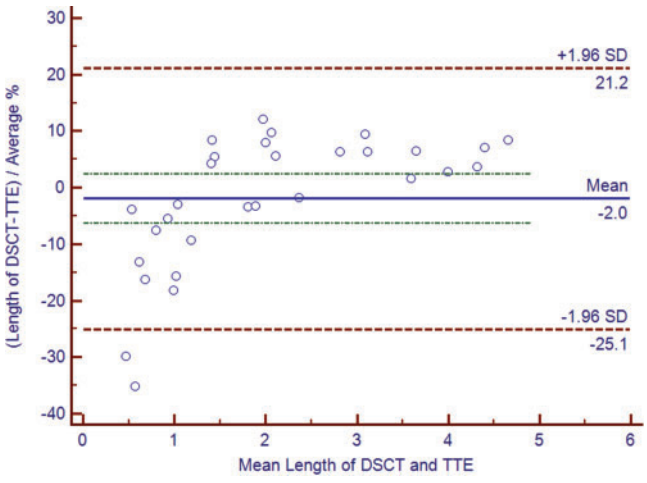

(b)

Figure 6. (a) Bland–Altman plot to show agreement between dual-source CT coronary angiography (DSCTCA) and transthoracic echocardiography (TTE) for measuring aneurysm diameter. (b) Bland–Altman plot to show agreement between DSCTCA and TTE for measuring aneurysm length.

Table 1. Radiation dose of different age groups

Age	$CTDI_{vol}$ (mGy)	DLP (mGy · cm)	Effective dose (mSv)
Under 4 months	0.49 ± 0.08	3.33 ± 0.58	0.32 ± 0.06
4 months to 1 year	0.77 ± 0.14	5.33 ± 0.87	0.35 ± 0.06
1 to 5 years	1.22 ± 0.26	8.86 ± 1.35	0.40 ± 0.06

$CTDI_{vol}$, CT volume dose index; DLP, dose–length product.

Discussion

Our study demonstrates the clinical feasibility of prospective ECG-triggered DSCTCA in children with coronary artery aneurysms due to KD. The location and size of coronary artery aneurysms described by DSCTCA were almost the same as those described by TTE, whereas DSCTCA showed more aneurysms in the distal coronary segments than TTE. Moreover, the effective radiation dose of our study was 0.36 ± 0.06 mSv.

KD is the most common cause of acquired heart disease in children [27]. Treatment with intravenous immunoglobulin at the onset of KD reduces the incidence of coronary lesions [28]. However, coronary artery aneurysms may rupture, thrombose, stenose or cause myocardial ischaemia if there is treatment failure or delay, so it is important to make an accurate diagnosis in the early stages of the disease. Slow blood flow in the dilated coronary artery may be a causative factor for thrombosis; evaluation of the precise size of aneurysms and confirmation of the presence of thrombosis play an important role in further treatment [29].

According to the recommendations of the American Heart Association [1, 8, 30], the long-term management of individual patients with KD is best considered by the risk stratification based upon their coronary artery involvement. The risk level of an isolated aneurysm in one coronary artery is different from that of multiple aneurysms in one coronary artery, and a previous study reported that 14% of the coronary aneurysms were located in the distal portion [31]; in our study, 2 out of 15 patients were assigned to a different risk level by CT angiography because of distal lesions. So it is important to carry out a thorough assessment of the whole coronary artery, including the distal coronary artery. TTE is the main imaging modality in children to evaluate proximal coronary artery disease and direction of flow [32, 33]. However, visualisation of the distal coronary artery segments using TTE is limited owing to deterioration of the acoustic window [20, 33, 34].

X-ray coronary angiography (XCA) is considered to be the gold standard for diagnosis and follow-up of coronary artery disease. However, because of the higher radiation dose, invasiveness, higher contrast material dose, the need for hospitalisation and potential complications (haematomas, dissections, vascular rupture, arrhythmias and death) [35, 36] the diagnostic role of XCA has largely been replaced by other advanced non-invasive imaging tools [33, 37]. MR angiography (MRA) has shown promise for visualisation of coronary arteries in children [33]. However, these approaches are time-consuming and general anaesthesia is needed [38]. Moreover, a low heart rate (ideally <100 bpm) and a regular heart beat interval are needed. In our study, the mean heart rate was 112 bpm, at which it is hard to acquire diagnostic images using MRA [33, 38].

With the development of CT technology, especially the application of DSCTCA with improved isotropic spatial (0.4 mm) and temporal (83 ms) resolution, cardiac CT examinations in children with thin coronary arteries (1 mm) and high heart rate are feasible [39, 40]. The findings were confirmed by both retrospective and prospective ECG-triggered CT angiography in children and infants with coronary artery deformities [2, 5, 7, 9, 12, 15–17, 20, 41]. A prospective ECG-triggered protocol was supposed to be as good as that of XCA [15, 16, 41]. However, ionising radiation is the inherent drawback of a CT scan. Children are much more radiosensitive than adults. A 1-year-old infant is 10–15 times as likely as a 50-year-old adult to develop a malignancy (leukaemia and solid cancers) from the same dose of radiation [42–44]. In addition, the effective radiation doses received by children are about 50% higher than those received by adults owing to their smaller body size and related attenuation [45]. Children also have a longer lifetime risk for developing radiation-induced cancers [46]. So minimising doses for paediatric CT examination is the ultimate goal. With an ECG-gated scan protocol, the coronary artery lesions can be depicted clearly with the fewest cardiac motion artefacts. A prospective ECG-triggered protocol, using the step-and-shoot technique, acquires data only at predefined time intervals during a preset phase of the cardiac cycle, and allows for significant dose reduction of up to 80% for complete examination of the coronary arteries with imaging quality comparable to retrospective techniques [16]. Low tube potential (80 kV) and a body-size-adapted CT protocol were used to lower the radiation exposure as far as possible in our study. In our study, the mean effective dose of all 19 cases was 0.36 ± 0.06 mSv (1 mSv is equivalent to the dose delivered by natural radiation over a 6-month period [14]).

Limitations

There are some limitations in the present study. First, a relatively small group of children with coronary artery disease due to KD was included; a further study with large samples is required. Second, information regarding myocardial ischaemia in children with coronary artery lesions due to KD should be evaluated in a further study. Third, XCA was not available in our study because the patients' guardians refused permission for invasive and risky examinations. So it was not feasible to evaluate the sensitivity, specificity, and positive and negative predictive values of DSCTCA in coronary artery lesions due to KD.

In conclusion, as an alternative diagnostic modality, prospective ECG-triggered DSCTCA is associated with excellent image quality and low radiation exposure and

has been proved useful for diagnosing infants and children with coronary artery aneurysms due to KD. Although far more coronary artery lesions were visualised by DSCTCA, this needs to be verified by XCA or a follow-up study.

References

1. Newburger JW, Takahashi M, Gerber MA, Gewitz MH, Tani LY, Burns JC, et al. Diagnosis, treatment, and long-term management of Kawasaki disease: a statement for health professionals from the Committee on Rheumatic Fever, Endocarditis, and Kawasaki Disease, Council on Cardiovascular Disease in the Young, American Heart Association. Pediatrics 2004;114:1708–33.
2. Goo HW, Park IS, Ko JK, Kim YH. Coronary CT angiography and MR angiography of Kawasaki disease. Pediatr Radiol 2006;36:697–705.
3. Greil GF, Stuber M, Botnar RM, Kissinger KV, Geva T, Newburger JW, et al. Coronary magnetic resonance angiography in adolescents and young adults with Kawasaki disease. Circulation 2002;105:908–11.
4. Mavrogeni S, Papadopoulos G, Douskou M, Kaklis S, Seimenis I, Baras P, et al. Magnetic resonance angiography is equivalent to X-ray coronary angiography for the evaluation of coronary arteries in Kawasaki disease. J Am Coll Cardiol 2004;43:649–52.
5. Xing Y, Wang H, Yu X, Chen R, Hou Y. Assessment of coronary artery lesions in children with Kawasaki disease: evaluation of MSCT in comparison with 2-D echocardiography. Pediatr Radiol 2009;39:1209–15.
6. O'Connor MJ, Saulsbury FT. Incomplete and atypical Kawasaki disease in a young infant: severe, recalcitrant disease. Clin Pediatr 2007;46:345–8.
7. Arnold R, Ley S, Ley-Zaporozhan J, Eichhorn J, Schenk JP, Ulmer H, et al. Visualization of coronary arteries in patients after childhood Kawasaki syndrome: value of multidetector CT and MR imaging in comparison to conventional coronary catheterization. Pediatr Radiol 2007;37:998–1006.
8. Newburger JW, Takahashi M, Gerber MA, Gewitz MH, Tani LY, Burns JC, et al. Diagnosis, treatment, and long-term management of Kawasaki disease: a statement for health professionals from the Committee on Rheumatic Fever, Endocarditis and Kawasaki Disease, Council on Cardiovascular Disease in the Young, American Heart Association. Circulation 2004;110:2747–71.
9. Chao BT, Wang XM, Wu LB, Chen J, Cheng ZP, Wu DW, et al. The diagnostic value of dual-source CT in Kawasaki disease. Chin Med J (Engl) 2010;123:670–4.
10. Ben Saad M, Rohnean A, Sigal-Cinqualbre A, Adler G, Paul JF. Evaluation of image quality and radiation dose of thoracic and coronary dual-source CT in 110 infants with congenital heart disease. Pediatr Radiol 2009;39:668–76.
11. Young C, Taylor AM, Owens CM. Pediatric cardiac computed tomography: a review of imaging techniques and radiation dose consideration. Eur Radiol 2011;21: 518–29.
12. Peng Y, Zeng J, Du Z, Sun G, Guo H. Usefulness of 64-slice MDCT for follow-up of young children with coronary artery aneurysm due to Kawasaki disease: initial experience. Eur J Radiol 2009;69:500–9.
13. Tsai IC, Chen MC, Jan SL, Wang CC, Fu YC, Lin PC, et al. Neonatal cardiac multi-detector row CT: why and how we do it. Pediatr Radiol 2008;35:438–51.
14. Paul JF, Rohnean A, Elfassy E, Sigal-Cinqualbre A. Radiation dose for thoracic and coronary step-and-shoot CT using a 128-slice dual-source machine in infants and small children with congenital heart disease. Pediatr Radiol 2011;41:244–9.
15. Cheng Z, Wang X, Duan Y, Wu L, Wu D, Chao B, et al. Low-dose prospective ECG-triggering dual-source CT angiography in infants and children with complex congenital heart disease: first experience. Eur Radiol 2010;20:2503–11.
16. Jin KN, Park EA, Shin CI, Lee W, Chung JW, Park JH. Retrospective versus prospective ECG-gated dual-source CT in pediatric patients with congenital heart diseases: comparison of image quality and radiation dose. Int J Cardiovasc Imaging 2010;26:S63–73.
17. Huang MP, Liang CH, Zhao ZJ, Liu H, Li JL, Zhang JE, et al. Evaluation of image quality and radiation dose at prospective ECG-triggered axial 256-slice multi-detector CT in infants with congenital heart disease. Pediatr Radiol 2011;41:858–66.
18. Awai K, Hiraishi K, Hori S. Effect of contrast material injection duration and rate on aortic peak time and peak enhancement at dynamic CT involving an injection protocol with dose tailored to patient weight. Radiology 2004; 230:142–50.
19. Yanaga Y, Awai K, Nakaura T, Utsunomiya D, Oda S, Hirai T, et al. Contrast material injection protocol with the dose adjusted to the body surface area for MDCT aortography. AJR Am J Roentgenol 2010;194:903–8.
20. Chu WC, Mok GC, Lam WW, Yam MC, Sung RY. Assessment of coronary artery aneurysms in pediatric patients with Kawasaki disease by multidetector row CT angiography: feasibility and comparison with 2D echocardiography. Pediatr Radiol 2006;36:1148–53.
21. Swaye PS, Fisher LD, Litwon P, Vignola PA, Judkins MP, Kemp HG, et al. Aneurysmal coronary artery disease. Circulation 1983;67:134–8.
22. Kayiran SM, Dindar A, Gurakan B. An evaluation of children with Kawasaki disease in Istanbul: a retrospective follow-up study. Clinics (Sao Paulo) 2010;65:1261–5.
23. Shrimpton PC, Hillier MC, Lewis MA, Dunn M. National survey of doses from CT in the UK: 2003. Br J Radiol 2006;79:968–80.
24. Pache G, Grohmann J, Bulla S, Arnold R, Stiller B, Schlensak C, et al. Prospective electrocardiography-triggered CT angiography of the great thoracic vessels in infants and toddlers with congenital heart disease: feasibility and image quality. Eur J Radiol 2011;80:e440–5.
25. American Association of Physicists in Medicine. The measurement, reporting, and management of radiation dose in CT. AAPM Report No. 95. College Park, MD: AAPM; 2008. Available from: www.aapm.org/pubs/reports/rpt_96.pdf
26. Kundel HL, Polansky M. Measurement of observer agreement. Radiology 2003;228:303–8.
27. Park YW, Han JW, Park IS, Kim CH, Yun YS, Cha SH, et al. Epidemiologic picture of Kawasaki disease in Korea, 2000–2002. Pediatr Int 2005;47:382–7.
28. Sittiwangkul R, Pongprot Y, Silvilairat S, Phornphutkul C. Delayed diagnosis of Kawasaki disease: risk factors and outcome of treatment. Ann Trop Paediatr 2011;31:109–14.
29. Papadakis M, Mangina A, Cotileas P, Demopoulos V, Voudris V, Pavlides G, et al. Documentation of slow coronary flow by TIMI frame count in patients with coronary artery ectasia. Am J Cardiol 2001;88:1030–2.
30. Rowley AH, Shulman ST. Pathogenesis and management of Kawasaki disease. Expert Rev Anti Infect Ther 2010; 8:197–203.
31. Kuribayashi S, Ootaki M, Tsuji M, Matsuyama S, Iwasaki H, Oota T. Coronary angiographic abnormalities in mucocutaneous lymph node syndrome: acute findings and long-term follow-up. Radiology 1989;172:629–33.
32. Hiraishi S, Misawa H, Takeda N, Horiguchi Y, Fujino N, Ogawa N, et al. Transthoracic ultrasonic visualization of coronary aneurysm, stenosis and occlusion in Kawasaki disease. Heart 2000;83:400–5.

33. Walsh R, Nielsen JC, Ko HH, Sanz J, Srivastava S, Parness IA, et al. Imaging of congenital coronary artery anomalies. Pediatr Radiol 2011;41:1526–35.
34. Mavrogeni S, Papadopoulos G, Karanasios E, Cokkinos DV. How to image Kawasaki disease: a validation of different imaging techniques. Int J Cardiol 2008;124:27–31.
35. Vitiello R, McCrindle BW, Nykanen D, Freedom RM, Benson LN. Complications associated with pediatric cardiac catheterization. J Am Coll Cardiol 1998;32:1433–40.
36. Kennedy JW, Baxley WA, Bunnel IL, Gensini GG, Messer JV, Mudd JG, et al. Mortality related to cardiac catheterization and angiography. Catheter Cardiovasc Diagn 1982;8:323–40.
37. Siripornpitak S, Pornkul R, Khowsathit P, Layangool T, Promphan W, Pongpanich B. Cardiac CT angiography in children with congenital heart disease. Eur J Radiol 2011; in press. E-pub ahead of print December 2011. DOI: 10.1016/j.ejrad.2011.11.042
38. Beerbaum P, Sarikouch S, Laser KT, Greil G, Burchert W, Körperich H. Coronary anomalies assessed by whole-heart isotropic 3D magnetic resonance imaging for cardiac morphology in congenital heart disease. J Magn Reson Imaging 2009;29:320–7.
39. Brodoefel H, Burgstahler C, Tsiflikas I, Reimann A, Schroeder S, Claussen CD, et al. Dual-source CT: effect of heart rate, heart rate variability, and calcification on image quality and diagnostic accuracy. Radiology 2008;247:346–55.
40. Chen SJ, Lee WJ, Lin MT, Liu KL, Wang JK, Lue HC. Coronary artery diameters in infants and children with congenital heart disease as determined by computed tomography. Am J Cardiol 2007;100:1696–701.
41. Walsh R, Nielsen JC, Ko HH, Sanz J, Srivastavs S, Parness IA, et al. Imaging of congenital coronary artery anomalies. Pediatr Radiol 2011;41:1526–35.
42. Hall EJ. Lessons we have learned from our children: cancer risks from diagnostic radiology. Pediatr Radiol 2002;32:700–6.
43. Wakeford R. The cancer epidemiology of radiation. Oncogene 2004;23:6404–284.
44. Brenner DJ, Elliston CD, Hall EJ, Berdon WE. Estimated risks of radiation-induced fatal cancer from pediatric CT. AJR Am J Roentgenol 2001;176:289–96.
45. Huda W. Dose and image quality in CT. Pediatr Radiol 2002;32:709–13.
46. Chodick G, Ronckers CM, Shalev V, Ron E. Excess lifetime cancer mortality risk attributable to radiation exposure from computed tomography examinations in children. Isr Med Assoc J 2007;9:584–7.